

pubs.acs.org/JPCC Article

Interfacial Properties of Water on Hydrogenated and Fluorinated Graphene Surfaces: Parametrization of Nonbonded Interactions

Amir Taqieddin, Mohammad Heiranian, and Narayana R. Aluru*



Cite This: J. Phys. Chem. C 2020, 124, 21467-21475



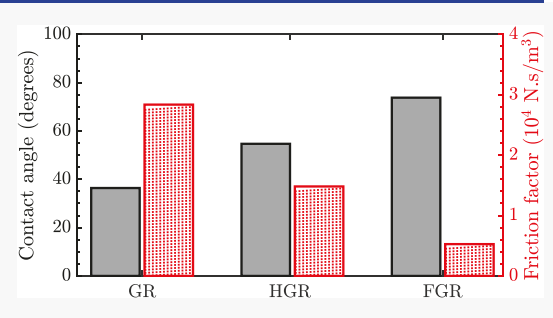
ACCESS

Metrics & More

Article Recommendations

3 Supporting Information

ABSTRACT: The properties of water interfacing with functionalized two-dimensional (2D) materials play a crucial role in the design and development of high-performance nanofluidic devices. Developing non-bonding force field parameters that can be used in molecular dynamics simulations allows researchers to study and understand the interfacial properties at the molecular scale. Here, we use high-level ab initio simulations based on the random-phase approximation method to develop force field parameters for the interaction of water with hydrogenated/fluorinated graphene surfaces. By performing molecular dynamics simulations based on the force fields developed here, hydrogenated and fluorinated graphene surfaces are shown to be more hydrophobic compared



to pristine graphene. Even though hydrogenated and fluorinated graphene surfaces having similar geometries, the fluorinated graphene has higher hydrophobicity due to its unique chemistry. The increase in the surface hydrophobicity leads to a decrease in the interfacial density and an increase in the slip length of water. Finally, we use first-principle simulations to show that a large decrease in the surface energy of the hydrogenated and the fluorinated graphene is the primary cause of their stronger hydrophobicity compared to pristine graphene.

1. INTRODUCTION

The successful exfoliation of graphene monolayer has brought a tremendous attention to the integration of two-dimensional (2D) materials into nanofluidic devices with many applications including water desalination, ^{2,3} energy harvesting, ^{4,5} photocatalvsis. ⁶ separation, ⁷ and biological sensing. ^{8,9} The 2D catalysis,⁶ separation,⁷ and biological sensing.^{8,9} The 2D material surfaces directly interact with water;^{2–9} therefore, understanding the interfacial properties at the water-solid interfaces is key to engineer these nanofluidic devices. The interfacial properties are strongly dictated by the properties of the 2D material surfaces (e.g., being hydrophilic or hydrophobic). The hydrophilicity or the hydrophobicity of a surface can be quantified by measuring the wetting contact angle formed by a water droplet on the target solid surface. The wetting properties of graphene have been intensively studied using theoretical and experimental investigations. The wetting contact angle of graphene can be tuned by either electrically or chemically doping the graphene surface. 14-18 Electrical doping works by imposing an electrical field on the surface of graphene. However, the imposed electric field could also alter the water properties such as the dipole orientation at the graphene interface since water is a polar molecule. 19 Alternatively, chemical modification via hydrogenation or fluorination can be used to tailor the wetting contact angle²⁰ or hydrophobicity of graphene.

Hydrogenated graphene (HGR) and fluorinated graphene (FGR) are chemical derivatives of graphene. The simplicity and reproducibility of forming these chemical

modifications have enabled investigation of the properties of HGR and FGR surfaces. 20-26 The nanotribological and electronic structure properties of HGR and FGR surfaces differ from that of pristine graphene (GR). 24-26 Further, unlike GR which is characterized by sp²-hybridization and a zero band gap, both HGR and FGR have sp³-hybridization resulting in a band gap opening. Having different surface chemistry compared to GR, HGR, and FGR possess different wetting properties as well.²⁰ Experimental measurements have shown somewhat inconsistent behavior as the water wetting angle on HGR has been shown to be both lower²⁰ and higher²⁷ compared to the wetting angle on GR. These contradictory observations are possibly due to different experimental conditions (i.e., different substrates, different types, and densities of contamination) or the hydrogenation concentration (fully HGR versus chair HGR).²³ On the other hand, FGR was experimentally shown to have a wetting contact angle larger than that of the measured angle on GR surface suggesting that FGR is a more hydrophobic surface compared to GR. 20,28,29 Theoretical and computational studies on the

Received: June 30, 2020 Revised: September 4, 2020 Published: September 9, 2020





wetting properties of HGR and FGR, however, are limited due to the lack of accurate force field (FF) parameters that can describe the interactions between the chemically modified graphene-based surfaces and water molecules. Accurate FF parameters are needed not only to address the wetting properties of HGR and FGR but also to predict other interfacial properties of water (e.g., the density profile and slip length). In addition, accurate FF parameters-based molecular dynamics (MD) simulations will help investigate possible usage of HGR and FGR surfaces in different nanofluidic applications. Therefore, it is important to establish high-accuracy FF parameters that allow accurate MD simulations of nanofluidic systems using HGR and FGR surfaces.

Developing MD FF parameters to describe both van der Waals (vdW) and Coulombic interactions requires the employment of accurate first-principle approaches. In fact, the accuracy of the FF parameters directly follows the fidelity of the first-principle method used to develop these parameters. The random-phase approximation (RPA) method 30,31 is one of the accurate ab initio methods. RPA provides an explicit approach to account for the electron-electron interactions via computing the correlation energy of many-electron systems.³² The explicit description of the correlation energy provides a better description of the vdW interactions.³³ Therefore, the RPA method is considered at the top of Jacob's ladder of density functional approximations.³⁴ Prior work has shown that when the FF parameters have been developed using RPA calculations, they are able to describe the experimentally measured properties. 13,33,35,36

In this work, we begin by developing the FF parameters using the RPA method to describe the interactions between HGR/FGR surfaces and water molecules. Then, we use the FF parameters in MD simulations to predict the interfacial properties of water on HGR and FGR surfaces. The computed properties include the contact angle, density profile, and slip length. In the final section, we study the surface energy and the electronic structure of GR, HGR, and FGR surfaces through first-principle simulations to better understand the wetting behavior. The aim of this work is to understand the wetting and interfacial properties of water at HGR and FGR interfaces and to provide the scientific community with accurate FF parameters that describe the interactions of water molecules with the 2D HGR and FGR surfaces.

2. METHODOLOGY FOR DEVELOPMENT OF FF PARAMETERS

To develop the FF parameters between water molecules and the HGR/FGR surface, we use the RPA method with the adiabatic-connection fluctuation-dissipation theorem (ACFDT)^{37–39} to describe the electron correlation energy. In this approach, the ground state energy of a system, $E_{\rm c}$ is given as the sum of the correlation energy, $E_{\rm c}$, and the exchange energy, $E_{\rm exx.}$ The expression for $E_{\rm c}$ is given by

$$E_{c} = \frac{1}{2\pi} \int_{0}^{\infty} \text{Tr}[\ln(1 - \chi^{0}(i\omega) + \chi^{0}(i\omega)V)]d\omega$$
 (1)

where Tr is the trace, χ^0 is the response function of the Kohn–Sham noninteracting system (independent particles), ω is the frequency, and V is the interacting potential operator (i.e., Coulomb kernel). $E_{\rm exx}$ is the Hartree–Fock energy, which also includes the kinetic, the Hartree, and the ion–electron interaction energies of the density functional theory (DFT) orbtials.³³ The generalized gradient approximation Perdew–

Burke–Ernzerhof (GGA-PBE)⁴⁰ functional is used to evaluate all of the initial calculations based on the Kohn–Sham noninteracting orbitals.

The RPA calculations are carried out using Vienna Ab initio Simulation Package (VASP). 41,42 Projector-augmented wave potentials were used in all of the simulations. More details on the simulation parameters and inputs are provided in the Appendix section. The potential energy surface between the HGR/FGR and water was evaluated using the RPA method by varying the separation distance and the orientation of the water molecule with respect to the HGR/FGR surface. The graphene-based surfaces and water were kept fixed. The optimized geometries of the HGR and FGR are obtained by minimizing the energy between the atoms using the DFT-D3 method. The coordinates of the optimized structures are provided in the Supporting Information Notes 1 and 2. The total interaction energy between the chemically modified graphene surface (HGR or FGR) and the water molecule, ΔE , is written as

$$\Delta E = E_{\text{graphene-water}} - E_{\text{graphene}} - E_{\text{water}}$$
 (2)

where $E_{\rm graphene-water}$, $E_{\rm graphene}$, and $E_{\rm water}$ are the energies of the HGR/FGR-water system, HGR/FGR surface, and the water molecule, respectively. Each energy term is calculated separately using the RPA method.

Prior to computing the potential energy surface between the graphene surface and water, we performed convergence studies to minimize the error (arising from the computational setup) in the RPA method. These studies include investigating the incomplete basis set, lattice constant in the aperiodic direction, supercell size and nonzero water coverage, and the finite kpoints.33,44 First, we increased the plane-wave energy cutoff from 400 to 600 eV to ensure the convergence of the basis set. Increasing the cutoff energy results in a change in ΔE of about 1 meV. Next, we tested the error associated with the nonphysical interactions in the aperiodic direction via increasing the vacuum size from 15 to 20 Å. When we increased the vacuum size, we found that ΔE shows a difference within 1 meV. The convergence of the exchange and correlation energies are determined by varying the combination of both the supercell size and the number of k-points to control the errors due to the supercell size, water coverage, and the finite k-points (see the Supporting Information, Figure S1). We selected a supercell size of 8×8 and k-points of 2×2 to compute the E_{exx} for which the estimated error is less than 1 meV. For the computation of E_c , we selected a supercell size of 2×2 and k-points of 8×8 , which provides an error of about 1 meV. Based on these error analyses, we estimate the maximum possible total error in computing ΔE to be 4 meV using the RPA method.

With the error being controlled, we computed the interactions between the graphene-based surface and the water molecule. The computed ΔE using the RPA method is used to evaluate the vdW interactions between the graphene-based surface and water as follows

$$\Delta E_{\rm vdW} = \Delta E - \Delta E_{\rm elec} \tag{3}$$

where $\Delta E_{
m vdW}$ and $\Delta E_{
m elec}$ are the vdW and electrostatic interaction energies. The $\Delta E_{
m elec}$ is modeled using the Coulomb's law

Table 1. Summary of the Optimized LJ Potential Parameters Between Water and the Functionalized Graphene

graphene surface	$\sigma_{ ext{C-O}} ext{ (Å)}$	$\varepsilon_{\mathrm{C-O}}$ (kcal/mol)	qc (e)	$\sigma_{i-\mathrm{O}}$ (Å)	ε_{i-O} (kcal/mol)	q_i (e)
hydrogenated $(i = H)$	3.436	0.0850	0.00	3.773	0.0607	0.00
fluorinated $(i = F)$	3.436	0.0850	0.56	4.231	0.0535	-0.56

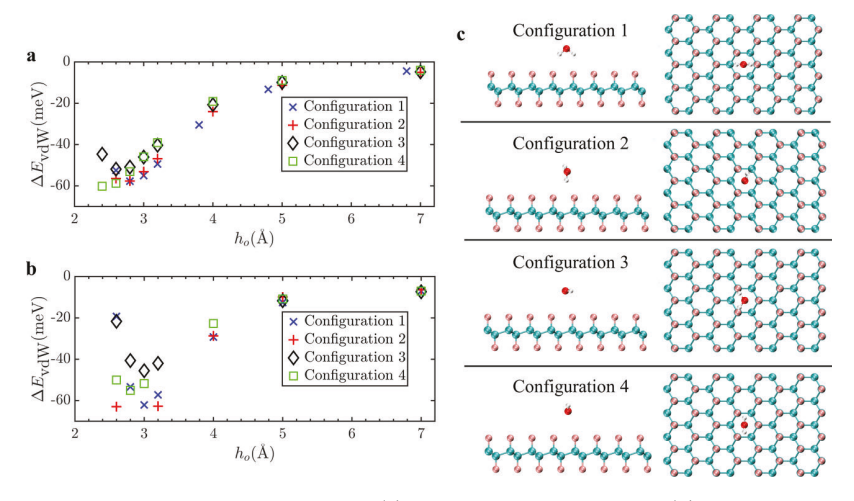


Figure 1. vdW interaction energy between one water molecule and (a) hydrogenated graphene, and (b) fluorinated graphene surfaces as a function of the separation distance, h_o , which is the shortest normal distance between the oxygen atom and the nearest hydrogen/fluorine layer, for four different water configurations. (c) Schematic of the top and side views of the four corresponding configurations (oxygen, hydrogen, carbon, and hydrogen/fluorine atoms are shown in red, white, cyan, and pink, respectively).

$$\Delta E_{\text{elec}} = \sum_{i \in \text{graphene}} \sum_{j \in \text{water}} \frac{q_i q_j}{r_{ij}}$$
(4)

where q_i and q_j are the partial charges of atoms i and j, respectively, and r_{ij} is the distance between atoms i and j. The partial charges of the HGR and FGR are determined using the Bader charge analysis based on the computed RPA charge densities. 45 The partial charges of water are obtained from the SPC/E water model.⁴⁶ The computed partial charges of both HGR and FGR are summarized in Table 1. By computing both ΔE and ΔE_{elec} , we determine ΔE_{vdW} , using eq 3, between HGR/FGR and water molecule for four different configurations. In all configurations, the water molecule is placed in the center of the graphene lattice (e.g., honeycomb). Prior work³³ has shown that changing the configuration of the water molecule away from the center of the lattice (e.g., honeycomb) will not significantly change the fitted LJ parameters. The computed $\Delta E_{\rm vdW}$ versus the separation distance between the graphene-based surface and the water molecule is shown in Figure 1. The computed ΔE_{vdW} profiles for the HGR-water interactions for the four different configurations are closely aligned as the HGR atoms have zero partial charges. However, for the FGR-water interactions, we see that the $\Delta E_{\rm vdW}$ profiles are not completely aligned as the FGR atoms have partial charges, which lead to different electrostatic interactions depending on the water orientation.

To obtain the FF parameters, $\Delta E_{\rm vdW}$ is characterized by the 12–6 Lennard-Jones (LJ) potential parameters as follows

$$\Delta E_{\text{vdW}} = \sum_{i \in \text{graphene}} \sum_{j \in \text{water}} 4\varepsilon_{ij} \left[\left(\frac{\sigma_{ij}}{r_{ij}} \right)^{12} - \left(\frac{\sigma_{ij}}{r_{ij}} \right)^{6} \right]$$
(5)

where ε_{ij} is the depth of the potential well of the vdW interactions between i and j atoms, and $2^{1/6} \sigma_{ij}$ is the position

of the potential well. The values of ε_{ij} and σ_{ij} can be determined by fitting the RPA data of $\Delta E_{\rm vdW}$. We neglect vdW interactions between the H atoms of the water molecule and the HGR/FGR surface since the O atom interaction is dominant compared to the H atoms. Excluding the H atoms vdW interactions should not affect the accuracy of the obtained FF parameters as the parametrization matches the computed $\Delta E_{\rm vdW}$ potential. Therefore, the simplified form of the 12–6 LJ interactions can be rewritten as

$$\Delta E_{\text{vdW}} = \sum_{i \in \text{graphene}} 4\varepsilon_{iO} \left[\left(\frac{\sigma_{iO}}{r_{iO}} \right)^{12} - \left(\frac{\sigma_{iO}}{r_{iO}} \right)^{6} \right]$$
(6)

where only four parameters need to be fit for each surface such that the i atom is either C or H for the HGR surface and is either C or F for the FGR surface.

Using Boltzmann averaging for the vdW interactions of the four different water configurations, we fit the LJ parameters using the least-squares fitting method. The fitted parameters are summarized for both HGR and FGR surfaces in Table 1. It should be noted that these parameters are developed based on the SPC/E model of water. 46 Also, the interaction parameters between the C and O atoms, for both HGR and FGR surfaces, are set to the previously obtained interaction parameters. This simplification is taken to reduce the fitting uncertainty. In fact, we found that changing the LJ parameters between the C and O atoms leads to a small variation in the LJ parameters between the H/F and O atoms because the later interactions are dominant compared to the C-O interactions (H/F atoms partially screen the carbon atoms). We computed the wetting contact angles of water on the HGR and FGR surfaces using molecular dynamics simulations using the LJ parameters developed in this work. The computation of the wetting contact angle is discussed next.

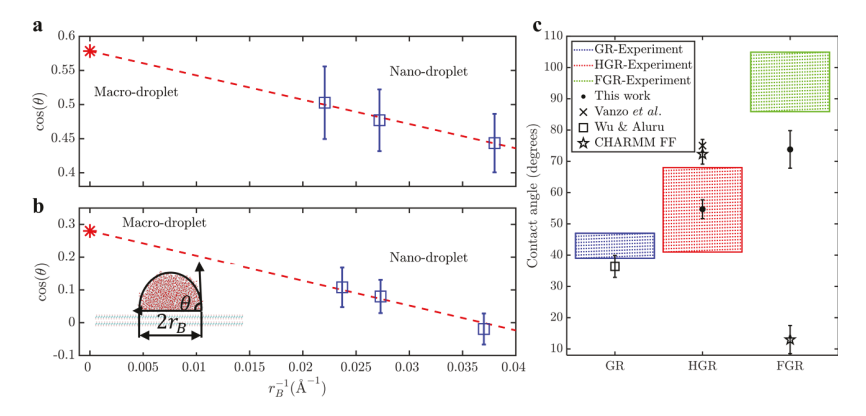


Figure 2. (a, b) Water contact angles on two layers of clean functionalized graphene surface for (a) hydrogenated graphene, and (b) fluorinated graphene where the angles in the nanodroplet region (blue symbols) are computed using the optimized LJ parameters and the macrodroplet angle (red curve and the symbol) is extrapolated using the Young's equation. (c) Comparison between the measured 10,20,28 and computed 13,48 contact angles from previous work and in this work for different graphene surfaces.

3. RESULTS AND DISCUSSION

3.1. Modeling the Wetting Contact Angles. Water contact angles on the HGR and FGR surfaces have been reported in several experimental measurements.^{20,27,28} Son et al. 20 reported the water contact angle on FGR, GR, and HGR surfaces to be 95 \pm 5°, 82 \pm 4°, and 42 \pm 2°, respectively. The reported measurements show that FGR is the most hydrophobic surface followed by GR and HGR surfaces. On the other hand, the experiment conducted by Zheng et al.27 showed that HGR is more hydrophobic compared to GR, where the water contact angle on HGR is measured to be 100°. Both Prydatko et al. 10 and Russo and Passmore 47 showed that exposing pristine graphene to H₂ plasma to produce hydrogenated graphene decreases the contact angle of water as the plasma tends to clean the surface contamination. Further, Prydatko et al. 10 showed that the change in the contact angle is negligible upon exposing a free-standing graphene to H₂ plasma. Lim and Ju²⁸ measured contact angles of 66.7 and 104.9° on GR and FGR, respectively. Vanzo et al.⁴⁸ performed MD simulations using OPLS-AA FF parameters to compute the water contact angle on a monolayer of GR and HGR. The simulation results showed that HGR is more hydrophobic compared to GR, where the contact angles on each surface are 75 and 73°, respectively. Measurements of the wetting contact angle are very sensitive to the measuring environments and conditions such as the presence of air contamination. 10,49-51 The water contact angle on clean GR is experimentally found to be 37-44°. 10,49,52 Wu and Aluru 13 developed FF parameters using the RPA method to describe the interactions between water and GR. They theoretically predicted the water contact angle on GR to be $36.4 \pm 3.5^{\circ}$. Their simulations show that the developed FF parameters using the RPA method can accurately recover the experimental wetting properties for clean GR. They also reported that computing the contact angle on a monolayer could produce an appreciably larger contact angle compared to that in double-layer graphene and beyond.

In this section, we use the LJ parameters developed using the RPA method to compute the water contact angle on two layers of HGR and FGR surfaces. The MD simulations are done using the LAMMPS⁵³ package (see the Appendix section for further details). We place a water box on top of the graphene-based layers with different number of water molecules, $n_{\rm w}$, to compute radius, $r_{\rm B}$, and the contact angle, θ , of the nanodroplet formed on the surface. The computed $r_{\rm B}$

and θ values are then used to extrapolate to the macroscopic droplet contact angle, θ_∞ , using the Young's equation, which is given by

$$\cos (\theta) = \cos (\theta_{\infty}) - \frac{\tau}{\gamma_{LV}} r_{B}^{-1}$$
(7)

where τ is the line tension and $\gamma_{\rm LV}$ is the water liquid—vapor surface tension. The linear relation between $\cos{(\theta)}$ and $r_{\rm B}^{-1}$ in eq 7 is used to extrapolate the value of $\cos{(\theta_{\infty})}$ when $r_{\rm B}^{-1}$ goes to zero for macroscopic droplets. This procedure of computing θ_{∞} is employed previously in several theoretical works. Experimentally, it is not possible to control the water droplet size by tuning $n_{\rm w}$; therefore, the computed θ_{∞} allows for a direct comparison between the MD simulations and the experimental measurements. The computed $\cos{(\theta)}$ values using MD versus $r_{\rm B}^{-1}$ of different $n_{\rm w}$ are shown in Figure 2 for both HGR and FGR surfaces. The extrapolated values of θ_{∞} are summarized in Table 2 for each graphene-based surface.

Table 2. Summary of the Computed Interfacial Properties of Water at the Interface of Pristine and Functionalized Graphene

graphene surface	$ heta_{\infty}^{ heta}$ (\deg)	$ ho_{ m water}$ (g/cm³) at the interface	$\lambda \left(N \cdot s/m^3\right)$	$\binom{l_{\mathrm{slip}}}{(\mathrm{nm})}$
pristine	36.4	3.34	2.837×10^{4}	25.7
hydrogenated	54.7	1.94	1.482×10^4	49.2
fluorinated	73.8	1.52	5.269×10^{3}	138.3

The evaluated θ_{∞} of GR, HGR, FGR are 36.4°, 54.7°, and 73.8°, which shows that both HGR and FGR are more hydrophobic compared to GR. This observation, which qualitatively agrees with the previous experimental and computational work, 20,27,28,48 can be supported by understanding the surface energy and electrostatic interactions between the graphene-based surface and water as discussed later in the manuscript. Figure 2 shows a quantitative comparison between the experimentally measured 10,20,28 and the computed 48 contact angles, including results from previous work, for both HGR and FGR surfaces. The computed contact angles between water and GR or HGR using the LJ parameters developed in this work by the RPA approach agree well with the experimentally measured contact angle between water and the corresponding free-standing graphene surfaces. 10 However,

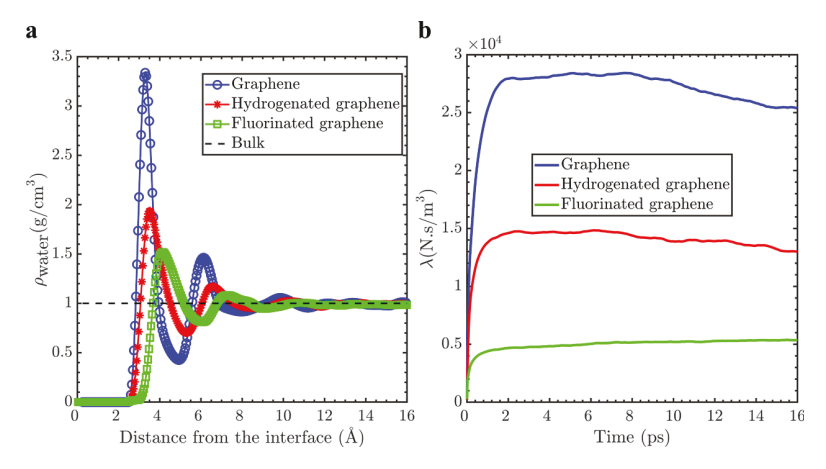


Figure 3. (a) Density profile of water as a function of the distance from the graphene surface, and (b) the integral of the force autocorrelation function (FACF) for pristine graphene, hydrogenated graphene, and fluorinated graphene.

we see a discrepancy between our computed contact angle and the experimentally measured contact angle for water and FGR surface. The discrepancy is due to dissimilar conditions between the simulations and the experiment for the water-FGR interactions. In simulations, we considered a freestanding FGR surface in vacuum and at present, to our knowledge, there is no experimental data for this case. Therefore, the main reason behind the discrepancy is the presence of a substrate and possible contamination in the experiment, which can strongly change the measured contact angle. 10,13 Further, the structure variation of the FGR surface (e.g., the FGR surface considered in simulations has fluorine atoms on both sides, whereas in the experiment, 55 the contact angle is measured for the chair FGR, where the fluorine atoms are placed on one side of the surface) can be another possible reason behind this discrepancy.

We also computed the contact angles of water on HGR and FGR surfaces using CHARMM FF (for details see the Supporting Information, Note 5).⁵⁶ The comparison shows that our contact angle of water on HGR surface is within the experimental range (better prediction compared to the OPLS-AA48 and CHARMM⁵⁶ FF models), and the contact angle on FGR surface is within an acceptable error from the experimental range that is associated with the different measurement conditions such as the presence of contamination and the substrate effects as previously discussed (see the Supporting Information, Table S1 for a detailed comparison). We should highlight that CHARMM FF parameters underestimate the contact angle of water on FGR compared to LJ parameters developed in this work, which result in a much closer contact angle to that of the experimental measurements. The degree of hydrophobicity in different functionalized surfaces changes the interfacial properties such as the density and the friction factor. In the next section, we use MD simulations to predict the interfacial density and friction factor of water for graphene-based surfaces considered in this work.

3.2. Interfacial Density and Friction Factor. The wetting characteristics of the interface dictate the water structure affecting the static and dynamic properties of the water at the interface. In this section, we perform equilibrium MD simulations using the FF parameters developed in this work to understand the water structure at the interface of GR/HGR/FGR surfaces. We place a water box of ~7130 water molecules on top of the graphene-based monolayer. The

simulation details are discussed in the Appendix section. The computed average density profiles of water, $\rho_{\rm water}$ on GR, HGR, and FGR are shown in Figure 3. While the profiles of $\rho_{\rm water}$ are qualitatively similar for the three different systems, $\rho_{\rm water}$ near the interface exhibits a considerable variation. The peak values of $\rho_{\rm water}$ at the interface of GR, HGR, and FGR are summarized in Table 2. FGR surface shows high repulsion to water with an interfacial density of 1.54 g/cm³ compared to the interfacial densities of 1.94 and 3.34 g/cm³ for HGR and GR, respectively. The trend in the interfacial peak density values follows the trend of the computed wetting contact angles showing the highest water repulsion at the FGR interface and lowest at the GR interface with the HGR interface having an intermediate value between FGR and GR.

We examined the slip length, $l_{\rm slip}$, which is a microscopic dynamic property that can be experimentally measured to quantify the flow dynamics. The $l_{\rm slip}$ can be calculated using the relation $l_{\rm slip} = \eta/\lambda$, where η is the dynamic viscosity of water and λ is the friction factor coefficient. To compute λ of water at the GR, HGR, and FGR interfaces, we employ the linear response theory using the data obtained from the same equilibrium MD simulations, which are carried out to compute $\rho_{\rm water}$ (see the Appendix section for further details). In the linear response theory, λ is obtained from the equilibrium fluctuations of $F_{\rm p}$ (the wall-fluid friction force parallel to the 2D surface) using the Green–Kubo relation as $^{59-61}$

$$\lambda = \lim_{t \to \infty} \left(\frac{1}{2Ak_{\rm B}T} \int_0^t \langle F_{\rm p}(t') \cdot F_{\rm p}(0) \rangle \mathrm{d}t' \right) \tag{8}$$

where t is the time, A is the interfacial area, $k_{\rm B}$ is the Boltzmann constant, and T is the temperature. The factor 2 in the denominator accounts for the averaging of two spatial dimensions parallel to the sheets. The Figure 3, the time integral in eq 8 as a function of time is shown for the GR, HGR, and FGR interfaces, where λ values are obtained from a constant line fitting to the plateaus (in Figure 3) between time t=0 and 16 ps.

The values of λ and $l_{\rm slip}$ (evaluated using the SPC/E water viscosity $\eta=0.729\times 10^{-3}~{\rm Pa\cdot s}$) are shown in Table 2. Our computed λ at the GR interface is $2.837\times 10^4~{\rm N\cdot s/m^3}$, which closely matches the value ($\approx 3\times 10^4~{\rm N\cdot s/m^3}$) reported by Tocci et al. Tocci et al. Tocci et al. Compared to the HGR and FGR lowest $l_{\rm slip}$ (highest λ) compared to the HGR and FGR

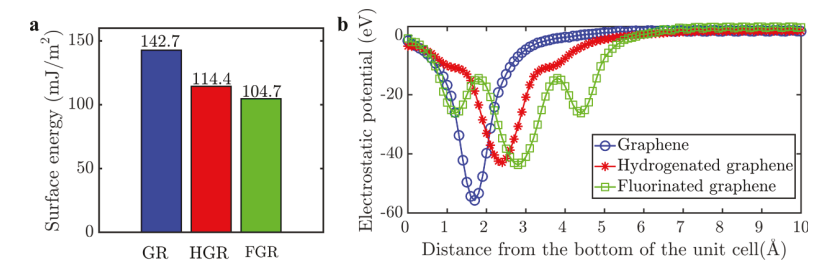


Figure 4. (a) Surface energy of graphene (blue), hydrogenated graphene (red), and fluorinated graphene (green), and (b) the electrostatic energy of a single layer of the graphene-based surface as a function of the distance measured from the bottom of the simulated unit cell. The data presented in this figure is obtained using DFT-D3 simulations.

interfaces suggesting that water molecules strongly adhere to the GR surface. On the other hand, FGR has the highest $l_{\rm slip}$ (lowest λ) due to the low attraction between the FGR surface and the water molecules. The values of $l_{\rm slip}$ and λ for HGR are intermediate between the values of the GR and FGR surfaces. Examining the trend in the $l_{\rm slip}$ between the different graphene-based surfaces supports the trend observed in the computed wetting contact angles, where FGR and HGR are shown to be more hydrophobic surfaces compared to GR. In the next section, we investigate the surface physics behind the increasing hydrophobicity of FGR and HGR using ab initio simulations.

3.3. Surface Energy. One of the key fundamental concepts to understand the wetting of a surface is the surface energy. 62-64 It is defined as the energy required to cleave a bulk sample into a new surface. This energy is considered as an excess energy since cleaving a surface out of bulk atoms leaves the atoms in the outmost layers with net forces and charges.⁶⁵ The higher the surface energy, the higher the reactivity of the surface as the surface interacts with the surrounding to minimize its energy. A surface minimizes its surface energy via either forming chemical bonds or adsorbing foreign molecules. Therefore, a surface with a high surface energy attracts more water molecules resulting in strong wetting (low contact angles). To understand the increase in the hydrophilicity of GR upon chemically modifying its surface with H/F atoms, we compute the surface energy of GR, HGR, and FGR surfaces using first-principle simulations.

For a 2D slab, the surface energy can be computed by taking the difference between the total energy of the formed slab and the equivalent energy of atoms in a bulk reference. Mathematically, the surface energy, E_{s} , can be written as

$$E_{\rm s} = \frac{1}{2A_{\rm s}} (E_n - N \times E_{\rm bulk}) \tag{9}$$

where A_s is the surface area of the 2D slab, E_n is the total energy of n layers of the 2D material, N is the number of atoms which form the n layers, and $E_{\rm bulk}$ is the bulk reference energy of the atoms. The factor 1/2 accounts for the two surface sides in the slab unit cell. We use VASP to compute E_s of our graphene-based surfaces using the DFT-D3 method. The computational details and the convergence of eq 9 are discussed in the Appendix section. Figure 4 shows the surface energies, E_s , of GR, HGR, and FGR surfaces. E_s decreases in the order of GR, HGR, and FGR. The chemical modification in both HGR and FGR form polar covalent bonds between C—H and C—F, respectively, resulting in a lower surface energy compared to the unmodified GR surface. Further, the electronegativity of the C—F bond is larger than the

electronegativity of the C–H bond. Therefore, the FGR surface has lower $E_{\rm s}$ compared to the HGR surface since FGR is more balanced with stronger bonds. It should be noted that the decrease in the surface energy from the GR to HGR is about 19.8%, and from GR to FGR is about 26.6%. Ko et al. ²⁴ reported a similar decrease in the adhesion energy from GR to HGR, and from GR to FGR which are 15 and 30%, respectively.

The computed surface energies, E_s , show that GR is the most attractive surface to adsorb molecules since it has the highest E_s . On the other hand, the FGR surface is the least attractive surface to adsorb molecules since it has the lowest E_s . Therefore, we expect GR to have the lowest wetting contact angle, highest density, and lowest slip length compared to the HGR and FGR surfaces. This observation is in agreement with our MD simulations of the wetting contact angles, interfacial density, and slip length. Additionally, the electrostatic potential due to the electrons and nuclei (see the Appendix section for further details) of the different graphene-based surfaces is shown in Figure 4. The electrostatic potential reveals that GR has the lowest potential, which means it is the most attractive surface. Although both HGR and FGR have almost the same magnitude of the attraction potential by the carbon atoms, FGR is more repulsive compared to HGR. The increased repulsion in FGR is due to the screened C atoms by F atoms, which is evident from the electrostatic potentials of FGR in Figure 4. These surface energy and electrostatic potential calculations using DFT-D3 provide additional support toward understanding the interfacial properties via the MD simulations, which are performed using the FF parameters computed using the RPA method.

4. CONCLUSIONS

In summary, we used the high-level RPA method to compute the interactions between HGR/FGR surfaces and water. The computed interaction energy is fitted to the LJ potential to develop the FF parameters. We carried out MD simulations using the FF parameters to compute the wetting contact angles of water on the HGR and FGR surfaces. Our MD simulations show that HGR and FGR surfaces are more hydrophobic compared to the GR surface. The increase in the hydrophobicity leads to a decrease in the interfacial density and increase in the slip length of water. The MD simulations showed that FGR has the lowest interfacial density and highest slip length compared to HGR and GR surfaces. To explain the increase in the hydrophobicity of the chemically modified graphene surfaces, HGR and FGR, we computed the surface energies of each surface. The DFT-D3 results show that FGR has the lowest surface energy, GR has the highest energy, and

HGR has a surface energy between the FGR and GR surface energies. As the surface energy increases, the hydrophobicity decreases since the surface becomes more attractive to adsorb water and minimize its surface energy. The FF parameters developed in this work and the understanding of the wetting characteristics of HGR and FGR surfaces will assist future investigation of possible usage of these surfaces in different nanofluidic devices. Further, these FF parameters will provide new opportunities to accurately determine interfacial properties of water at the interfaces of HGR and FGR such as the work of adhesion, transport properties of water in nanoconfined spaces (e.g., diffusion and permeation rates), and dielectric permittivity of water. It will also assist researchers in modeling aqueous solutions in biological systems, electroosmotic devices, and energy harvesting applications.

APPENDIX

Evaluation of the Interaction Energies Using the RPA Method

The RPA method is used to compute the total interaction energy between the HGR/FGR surface and water. We first obtained the relaxed structures of HGR and FGR using DFT-D3. The structure relaxation is carried out with a plane-wave energy cutoff of 400 eV. Projector-augmented wave pseudopotentials are used at the GGA-PBE level. The structures were relaxed until the maximum force between the atoms reached less than 0.01 eV/Å and the energy converged to a threshold of 10^{-6} eV using an 8 × 8 k-mesh. The vacuum level is kept to ~15 Å to ensure suppression of unphysical interactions in the aperiodic direction. The relaxed structures are provided in the Supporting Information Notes 1 and 2.

Once the optimized structures of HGR and FGR surfaces are obtained, we computed the total interaction energy between the water and the surface by changing the separation distance between the water and the surface and using four different orientations of a water molecule with respect to the 2D material surface. In the RPA simulations, we used a planewave energy cutoff of 400 eV with projector-augmented wave pseudopotentials at the GGA-PBE level. The energy threshold was kept to 10^{-6} eV with a vacuum level of ~15 Å. An energy of 272 eV was used to expand the response function in the plane waves. The number of bands was set to the maximum number of plane waves to ensure large number of empty bands. The size of the supercell and the number of k-mesh points were selected for the exchange and correlation energy calculations based on the performed convergence study as indicated in the main text and shown in the Supporting Information, Figure S1.

Wetting Contact Angle Simulations. The contact angles were computed using the LAMMPS package. We considered two layers of HGR and FGR in each system. Each layer has a dimension of $\sim 20 \times 20 \text{ nm}^2$ (with a vacuum of 2 nm in the aperiodic direction), which is large enough to suppress the interactions between the water droplets in the periodic images. The number of water molecules was varied as mentioned in the main text to capture the dependence of the contact angle on the droplet size. The water-surface systems were allowed to equilibrate for 4 ns using NVT ensemble. The Nosé–Hoover 66,67 thermostat with a time constant of 0.1 ps was used with a timestep of 1 fs and a temperature of 300 K. The initial simulation box was generated using PACKMOL. We used the extended simple point charge (SPC/E) water model

and constrained the water molecules using the SHAKE algorithm to maintain the rigidity of each molecule. The cutoff distance for LJ interactions was set to 1.4 nm and the long-range interactions were computed using the particle—particle—mesh (PPPM) method. Following the equilibration, we run the systems for another 6 ns to ensure sufficient statistics to compute the contact angles. All visualizations were done using the VMD software.

Interfacial Density and Friction Factor Simulations. To compute the interfacial density and the friction factor, we created a box of GR, HGR, or FGR monolayer with \sim 7130 water molecules on the top. Each layer has a graphene-based layer of \sim 5 \times 5 nm² with a vacuum space of 2 nm in the aperiodic direction. The water molecules were placed on the top of graphene using PACKMOL. A timestep of 2 fs was used in these simulations, and the systems were equilibrated for 2 ns using the NVT ensemble, followed by 18 ns production run to collect statistics. All other parameters that are used to describe the simulations are the same ones used in computing the contact angles. The density profile was averaged every 2 ps in the direction perpendicular to the graphene surface. The force autocorrelation function was integrated for a period of 100 ps.

Surface Energy and Electrostatic Potential Simulations. The surface energies of GR, HGR, and FGR were computed using VASP. We used the optimized structures that are generated for the RPA calculations. A plane-wave energy cutoff of 450 eV and projector-augmented wave pseudopotentials at the GGA-PBE level were used with an energy threshold of 10^{-6} eV and a vacuum level of ~ 15 Å. A 12×12 k-mesh was used to compute the surface energy. We varied the number of layers from 1 to 13 to ensure that the surface energies are converged to an error less than 300 meV. The bulk reference energy term in eq 9 is calculated by obtaining the slope of E_n versus N to avoid systematic numerical errors.

The average electrostatic potential, V(r), is computed for a monolayer of GR, HGR, or FGR using the following equation⁷¹

$$V(r) = \int dr' \frac{n(r')}{|r - r'|} + V_{loc}(r)$$
(10)

where the first term on the right-hand side is the Hartree potential, which accounts for the Coulomb interactions between an electron with the electron density, n(r), and the second term, $V_{\rm loc}(r)$, is the local potential that includes the interactions between the nuclei and the core electron.

ASSOCIATED CONTENT

Supporting Information

The Supporting Information is available free of charge at https://pubs.acs.org/doi/10.1021/acs.jpcc.0c05951.

Structure coordinates of the hydrogenated and fluorinated surfaces, and a comparison between the measured and computed contact angles of water on the hydrogenated and fluorinated surfaces (PDF)

AUTHOR INFORMATION

Corresponding Author

Narayana R. Aluru — Department of Mechanical Science and Engineering Beckman Institute for Advanced Science and Technology, University of Illinois at Urbana-Champaign, Urbana, Illinois 61801, United States; orcid.org/0000-

0002-9622-7837; Phone: +1 (217) 333-1180; Email: aluru@illinois.edu; http://aluru.mechse.illinois.edu/

Authors

Amir Taqieddin — Department of Mechanical Science and Engineering Beckman Institute for Advanced Science and Technology, University of Illinois at Urbana-Champaign, Urbana, Illinois 61801, United States; orcid.org/0000-0002-5743-7110

Mohammad Heiranian — Department of Mechanical Science and Engineering Beckman Institute for Advanced Science and Technology, University of Illinois at Urbana-Champaign, Urbana, Illinois 61801, United States;

orcid.org/0000-0002-2227-4948

Complete contact information is available at: https://pubs.acs.org/10.1021/acs.jpcc.0c05951

Notes

The authors declare no competing financial interest.

ACKNOWLEDGMENTS

This research was supported by the National Science Foundation (NSF) through the University of Illinois at Urbana-Champaign Materials Research Science and Engineering Center DMR-1720633. The simulations were performed using the Extreme Science and Engineering Discovery Environment (XSEDE) (supported by NSF Grant no. OCI1053575), Blue Waters (supported by NSF awards OCI-0725070, ACI-1238993 and the state of Illinois, and as of December, 2019, supported by the National Geospatial-Intelligence Agency), and Frontera computing project at the Texas Advanced Computing Center (supported by NSF Grant no. OAC-1818253).

REFERENCES

- (1) Novoselov, K. S.; Geim, A. K.; Morozov, S. V.; Jiang, D.; Zhang, Y.; Dubonos, S. V.; Grigorieva, I. V.; Firsov, A. A. Electric field effect in atomically thin carbon films. *Science* **2004**, *306*, 666–669.
- (2) Heiranian, M.; Farimani, A. B.; Aluru, N. R. Water desalination with a single-layer MoS, nanopore. *Nat. Commun.* **2015**, *6*, No. 8616.
- (3) Dervin, S.; Dionysiou, D. D.; Pillai, S. C. 2D nanostructures for water purification: graphene and beyond. *Nanoscale* **2016**, *8*, 15115–15131.
- (4) Feng, J.; Graf, M.; Liu, K.; Ovchinnikov, D.; Dumcenco, D.; Heiranian, M.; Nandigana, V.; Aluru, N. R.; Kis, A.; Radenovic, A. Single-layer MoS₂ nanopores as nanopower generators. *Nature* **2016**, 536, 197–200.
- (5) Yang, J.; Hu, X.; Kong, X.; Jia, P.; Ji, D.; Quan, D.; Wang, L.; Wen, Q.; Lu, D.; Wu, J.; et al. Photo-induced ultrafast active ion transport through graphene oxide membranes. *Nat. Commun.* **2019**, *10*. No. 1171.
- (6) Rahman, M. Z.; Kwong, C. W.; Davey, K.; Qiao, S. Z. 2D phosphorene as a water splitting photocatalyst: fundamentals to applications. *Energy Environ. Sci.* **2016**, *9*, 709–728.
- (7) Liu, G.; Jin, W.; Xu, N. Two-dimensional-material membranes: a new family of high-performance separation membranes. *Angew. Chem., Int. Ed.* **2016**, *55*, 13384–13397.
- (8) Zhu, C.; Du, D.; Lin, Y. Graphene-like 2D nanomaterial-based biointerfaces for biosensing applications. *Biosens. Bioelectron.* **2017**, *89*, 43–55.
- (9) Farimani, A. B.; Min, K.; Aluru, N. R. DNA base detection using a single-layer MoS₂. ACS Nano **2014**, 8, 7914–7922.
- (10) Prydatko, A. V.; Belyaeva, L. A.; Jiang, L.; Lima, L. M. C.; Schneider, G. F. Contact angle measurement of free-standing square-millimeter single-layer graphene. *Nat. Commun.* **2018**, *9*, No. 4185.

- (11) Taherian, F.; Marcon, V.; van der Vegt, N. F.; Leroy, F. What is the contact angle of water on graphene? *Langmuir* **2013**, *29*, 1457–1465.
- (12) Kozbial, A.; Li, Z.; Conaway, C.; McGinley, R.; Dhingra, S.; Vahdat, V.; Zhou, F.; D'Urso, B.; Liu, H.; Li, L. Study on the surface energy of graphene by contact angle measurements. *Langmuir* **2014**, 30, 8598–8606.
- (13) Wu, Y.; Aluru, N. R. Graphitic carbon-water nonbonded interaction parameters. *J. Phys. Chem. B* **2013**, *117*, 8802–8813.
- (14) Giovambattista, N.; Debenedetti, P. G.; Rossky, P. J. Effect of surface polarity on water contact angle and interfacial hydration structure. *J. Phys. Chem. B* **2007**, *111*, 9581–9587.
- (15) Ostrowski, J. H.; Eaves, J. D. The tunable hydrophobic effect on electrically doped graphene. *J. Phys. Chem. B* **2014**, *118*, 530–536.
- (16) Rafiee, J.; Rafiee, M. A.; Yu, Z. Z.; Koratkar, N. Superhydrophobic to superhydrophilic wetting control in graphene films. *Adv. Mater.* **2010**, 22, 2151–2154.
- (17) Rafiee, J.; Mi, X.; Gullapalli, H.; Thomas, A. V.; Yavari, F.; Shi, Y.; Ajayan, P. M.; Koratkar, N. A. Wetting transparency of graphene. *Nat. Mater.* **2012**, *11*, 217–222.
- (18) Shih, C. J.; Wang, Q. H.; Lin, S.; Park, K. C.; Jin, Z.; Strano, M. S.; Blankschtein, D. Breakdown in the wetting transparency of graphene. *Phys. Rev. Lett.* **2012**, *109*, No. 176101.
- (19) Song, F.; Ma, L.; Fan, J.; Chen, Q.; Lei, G.; Li, B. Q. Electrowetting of a nanoscale water droplet on a polar solid surface in electric fields. *Phys. Chem. Chem. Phys.* **2018**, *20*, 11987–11993.
- (20) Son, J.; Buzov, N.; Chen, S.; Sung, D.; Ryu, H.; Kwon, J.; Kim, S.; Namiki, S.; Xu, J.; Hong, S.; et al. Tailoring surface properties via functionalized hydrofluorinated graphene compounds. *Adv. Mater.* **2019**, *31*, No. e1903424.
- (21) Elias, D. C.; Nair, R. R.; Mohiuddin, T. M.; Morozov, S. V.; Blake, P.; Halsall, M. P.; Ferrari, A. C.; Boukhvalov, D. W.; Katsnelson, M. I.; Geim, A. K.; et al. Control of graphene's properties by reversible hydrogenation: evidence for graphane. *Science* **2009**, 323, 610–613.
- (22) Nair, R. R.; Ren, W.; Jalil, R.; Riaz, I.; Kravets, V. G.; Britnell, L.; Blake, P.; Schedin, F.; Mayorov, A. S.; Yuan, S.; et al. Fluorographene: a two-dimensional counterpart of Teflon. *Small* **2010**, *6*, 2877–2884.
- (23) Kashtiban, R. J.; Dyson, M. A.; Nair, R. R.; Zan, R.; Wong, S. L.; Ramasse, Q.; Geim, A. K.; Bangert, U.; Sloan, J. Atomically resolved imaging of highly ordered alternating fluorinated graphene. *Nat. Commun.* **2014**, *5*, No. 4902.
- (24) Ko, J.-H.; Kwon, S.; Byun, I.-S.; Choi, J. S.; Park, B. H.; Kim, Y.-H.; Park, J. Y. Nanotribological properties of fluorinated, hydrogenated, and oxidized graphenes. *Tribol. Lett.* **2013**, *50*, 137–144.
- (25) Kwon, S.; Ko, J. H.; Jeon, K. J.; Kim, Y. H.; Park, J. Y. Enhanced nanoscale friction on fluorinated graphene. *Nano Lett.* **2012**, *12*, 6043–6048.
- (26) Wang, L.-F.; Ma, T.-B.; Hu, Y.-Z.; Wang, H.; Shao, T.-M. Ab initio study of the friction mechanism of fluorographene and graphane. *J. Phys. Chem. C* **2013**, *117*, 12520–12525.
- (27) Zheng, L.; Li, Z.; Bourdo, S.; Watanabe, F.; Ryerson, C. C.; Biris, A. S. Catalytic hydrogenation of graphene films. *Chem. Commun.* **2011**, 47, 1213–1215.
- (28) Lim, T.; Ju, S. Control of graphene surface wettability by using CF₄ plasma. *Surf. Coat. Technol.* **2017**, 328, 89–93.
- (29) Bharathidasan, T.; Narayanan, T. N.; Sathyanaryanan, S.; Sreejakumari, S. S. Above 170° water contact angle and oleophobicity of fluorinated graphene oxide based transparent polymeric films. *Carbon* **2015**, *84*, 207–213.
- (30) Harl, J.; Kresse, G. Accurate bulk properties from approximate many-body techniques. *Phys. Rev. Lett.* **2009**, *103*, No. 056401.
- (31) Lebègue, S.; Harl, J.; Gould, T.; Angyan, J. G.; Kresse, G.; Dobson, J. F. Cohesive properties and asymptotics of the dispersion interaction in graphite by the random phase approximation. *Phys. Rev. Lett.* **2010**, *105*, No. 196401.

- (32) Eshuis, H.; Bates, J. E.; Furche, F. Electron correlation methods based on the random phase approximation. *Theor. Chem. Acc.* **2012**, 131, No. 1084.
- (33) Heiranian, M.; Wu, Y.; Aluru, N. R. Molybdenum disulfide and water interaction parameters. *J. Chem. Phys.* **2017**, *147*, No. 104706.
- (34) Perdew, J. P.; Ruzsinszky, A.; Tao, J.; Staroverov, V. N.; Scuseria, G. E.; Csonka, G. I. Prescription for the design and selection of density functional approximations: more constraint satisfaction with fewer fits. *J. Chem. Phys.* **2005**, *123*, No. 062201.
- (35) Hilder, T. A.; Yang, R.; Ganesh, V.; Gordon, D.; Bliznyuk, A.; Rendell, A. P.; Chung, S. H. Validity of current force fields for simulations on boron nitride nanotubes. *Micro Nano Lett.* **2010**, *5*, No. 150
- (36) Li, H.; Zeng, X. C. Wetting and interfacial properties of water nanodroplets in contact with graphene and monolayer boron-nitride sheets. *ACS Nano* **2012**, *6*, 2401–2409.
- (37) Gunnarsson, O.; Lundqvist, B. I. Exchange and correlation in atoms, molecules, and solids by the spin-density-functional formalism. *Phys. Rev. B* **1976**, *13*, 4274–4298.
- (38) Langreth, D. C.; Perdew, J. P. Exchange-correlation energy of a metallic surface: Wave-vector analysis. *Phys. Rev. B* **1977**, *15*, 2884–2901.
- (39) Harl, J.; Schimka, L.; Kresse, G. Assessing the quality of the random phase approximation for lattice constants and atomization energies of solids. *Phys. Rev. B* **2010**, *81*, No. 115126.
- (40) Perdew, J. P.; Burke, K.; Ernzerhof, M. Generalized gradient approximation made simple. *Phys. Rev. Lett.* **1996**, *77*, 3865–3868.
- (41) Kresse, G.; Hafner, J. Ab initio molecular dynamics for open-shell transition metals. *Phys. Rev. B* **1993**, *48*, 13115–13118.
- (42) Kresse, G.; Furthmuller, J. Efficient iterative schemes for ab initio total-energy calculations using a plane-wave basis set. *Phys. Rev.* B **1996**, *54*, 11169–11186.
- (43) Grimme, S.; Antony, J.; Ehrlich, S.; Krieg, H. A consistent and accurate ab initio parametrization of density functional dispersion correction (DFT-D) for the 94 elements H-Pu. *J. Chem. Phys.* **2010**, 132, No. 154104.
- (44) Wu, Y.; Wagner, L. K.; Aluru, N. R. Hexagonal boron nitride and water interaction parameters. *J. Chem. Phys.* **2016**, *144*, No. 164118.
- (45) Tang, W.; Sanville, E.; Henkelman, G. A grid-based Bader analysis algorithm without lattice bias. *J. Phys.: Condens. Matter* **2009**, 21, No. 084204.
- (46) Berendsen, H. J. C.; Grigera, J. R.; Straatsma, T. P. The missing term in effective pair potentials. *J. Phys. Chem. A* **1987**, *91*, 6269–6271.
- (47) Russo, C. J.; Passmore, L. A. Controlling protein adsorption on graphene for cryo-EM using low-energy hydrogen plasmas. *Nat. Methods* **2014**, *11*, 649–652.
- (48) Vanzo, D.; Bratko, D.; Luzar, A. Wettability of pristine and alkyl-functionalized graphane. *J. Chem. Phys.* **2012**, *137*, No. 034707.
- (49) Li, Z.; Wang, Y.; Kozbial, A.; Shenoy, G.; Zhou, F.; McGinley, R.; Ireland, P.; Morganstein, B.; Kunkel, A.; Surwade, S. P.; et al. Effect of airborne contaminants on the wettability of supported graphene and graphite. *Nat. Mater.* **2013**, *12*, 925–931.
- (50) Yiapanis, G.; Makarucha, A. J.; Baldauf, J. S.; Downton, M. T. Simulations of graphitic nanoparticles at air-water interfaces. *Nanoscale* **2016**, *8*, 19620–19628.
- (51) Andrews, J. E.; Sinha, S.; Chung, P. W.; Das, S. Wetting dynamics of a water nanodrop on graphene. *Phys. Chem. Chem. Phys.* **2016**, *18*, 23482–23493.
- (52) Schrader, M. E. Ultrahigh vacuum techniques in the measurement of contact angles. IV. Water on graphite (0001). *J. Phys. Chem. B* **1975**, *79*, 2508–2515.
- (53) Plimpton, S. Fast parallel algorithms for short-range molecular dynamics. *J. Comput. Phys.* **1995**, *117*, 1–19.
- (54) Werder, T.; Walther, J. H.; Jaffe, R. L.; Halicioglu, T.; Koumoutsakos, P. On the water—carbon interaction for use in molecular dynamics simulations of graphite and carbon nanotubes. *J. Comput. Phys. B* **2003**, *107*, 1345–1352.

- (55) Son, J.; Lee, J. Y.; Han, N.; Cha, J.; Choi, J.; Kwon, J.; Nam, S.; Yoo, K. H.; Lee, G. H.; Hong, J. Tunable wettability of graphene through nondestructive hydrogenation and wettability-based patterning for bioapplications. *Nano Lett.* **2020**, *20*, 5625–5631.
- (56) Vanommeslaeghe, K.; Hatcher, E.; Acharya, C.; Kundu, S.; Zhong, S.; Shim, J.; Darian, E.; Guvench, O.; Lopes, P.; Vorobyov, I.; Mackerell, A. D., Jr. CHARMM general force field: A force field for drug-like molecules compatible with the CHARMM all-atom additive biological force fields. *J. Comput. Chem.* **2010**, *31*, 671–690.
- (57) Tocci, G.; Joly, L.; Michaelides, A. Friction of water on graphene and hexagonal boron nitride from ab initio methods: very different slippage despite very similar interface structures. *Nano Lett.* **2014**, *14*, 6872–6877.
- (58) Bocquet, L.; Barrat, J.-L. Flow boundary conditions from nanoto micro-scales. *Soft Matter* **2007**, *3*, 685.
- (59) Bocquet, L.; Barrat, J. L. Hydrodynamic boundary conditions, correlation functions, and Kubo relations for confined fluids. *Phys. Rev. E* **1994**, *49*, 3079–3092.
- (60) Bocquet, L.; Barrat, J. L. On the Green-Kubo relationship for the liquid-solid friction coefficient. *J. Chem. Phys.* **2013**, *139*, No. 044704.
- (61) Zwanzig, R. Time-correlation functions and transport coefficients in statistical mechanics. *Annu. Rev. Phys. Chem.* **1965**, 16, 67–102.
- (62) Fowkes, F. M. Attractive forces at interfaces. *Ind. Eng. Chem. Res.* **1964**, *56*, 40–52.
- (63) Jańczuk, B.; Białlopiotrowicz, T. Surface free-energy components of liquids and low energy solids and contact angles. *J. Colloid Interface Sci.* **1989**, *127*, 189–204.
- (64) Good, R. J. A Thermodynamic derivation of Wenzel's modification of Young's equation for contact angles; together with a theory of hysteresis1. *J. Am. Chem. Soc.* **1952**, *74*, 5041–5042.
- (65) Singh-Miller, N. E.; Marzari, N. Surface energies, work functions, and surface relaxations of low-index metallic surfaces from first principles. *Phys. Rev. B* **2009**, 80, No. 235407.
- (66) Nosé, S. A unified formulation of the constant temperature molecular dynamics methods. *J. Chem. Phys.* **1984**, *81*, 511–519.
- (67) Hoover, W. G. Canonical dynamics: Equilibrium phase-space distributions. *Phys. Rev. A* **1985**, *31*, 1695–1697.
- (68) Martínez, L.; Andrade, R.; Birgin, E. G.; Martinez, J. M. PACKMOL: a package for building initial configurations for molecular dynamics simulations. *J. Comput. Chem.* **2009**, 30, 2157–2164
- (69) Buneman, O. Computer simulation using particles (R. W. Hockney and J. W. Eastwood). SIAM Rev. 1983, 25, 425–426.
- (70) Humphrey, W.; Dalke, A.; Schulten, K. VMD: visual molecular dynamics. *J. Mol. Graphics* **1996**, *14*, 33–38.
- (71) Sundararaman, R.; Ping, Y. First-principles electrostatic potentials for reliable alignment at interfaces and defects. *J. Chem. Phys.* **2017**, *146*, No. 104109.